Acta Biochimica Indonesiana

https://doi.org/10.32889/actabioina.228

RESEARCH ARTICLE

Open Access

Anti-obesity potential of *Eurycoma longifolia*: molecular docking and experimental validation in diet-induced obese rats

Dimas Ikhsan Airlangga[1*], Hanifa Rizky Rahmawati[2], Triawanti[1], Muhammad Alrizal Rahman[3]

[1]Biochemistry and Biomolecular Laboratory, Faculty of Medicine and Health Sciences, Lambung Mangkurat University, Banjarmasin, Indonesia

[2]AIDS. Toxoplasma, Opportunistic Disease and Malaria Research Group, Faculty of Medicine, Universitas Brawijaya, Malang, East Java, Indonesia

[3]Undergraduate Students, Undergraduate Medical Study Program, Faculty of Medicine and Health Sciences, Lambung Mangkurat University, Banjarmasin, Indonesia

[*]Corresponding author: dimasairlangga@ulm.ac.id

ABSTRACT

Background: Obesity is associated with hyperlipidemia and enhanced adipogenesis mediated by HMGR and GPDH enzymes. *Eurycoma longifolia* represents a potential natural therapeutic alternative to statins for obesity management.

Objective: To investigate the anti-obesity potential of *E. longifolia* compounds through HMGR and GPDH inhibition using integrated in silico and in vivo approaches.

Methods: Molecular docking was performed using AutoDock Vina to evaluate interactions between seven bioactive compounds and HMGR/GPDH proteins. Validation was confirmed by RMSD values below 2 Å. Binding affinities and dissociation constants were analyzed. In vivo study employed Wistar rats fed high-calorie, high-fat diet for 12 weeks, followed by four weeks of *E. longifolia* extract treatment at varying doses. Body weight and intra-abdominal fat were measured.

Results: Three compounds exhibited binding affinities equivalent to atorvastatin against HMGR (-8.4 kcal/mol). Four compounds demonstrated stronger affinity than metformin against GPDH. Extract administration significantly reduced intra-abdominal fat in a dose-dependent manner ($p = 0.000$).

Conclusion: *E. longifolia* compounds demonstrate dual inhibitory potential against HMGR and GPDH through computational modeling, with experimental validation confirming significant reduction in visceral adiposity in obese rats.

Keywords: molecular docking; HMGR inhibition; GPDH inhibition; *Eurycoma longifolia*; visceral adiposity

Introduction

Obesity is a multifactorial metabolic disorder associated with increased risk for hypertension, type 2 diabetes mellitus, cardiovascular disease, stroke, and various cancers [1]. The World Health Organization reported that approximately 800 million people worldwide had obesity in 2016, with projections estimating this will affect 167 million individuals by 2025 [2]. In the Asia-Pacific region, obesity prevalence is predicted to increase through 2030, particularly in Southeast and South Asia [3]. In Indonesia, national adult obesity prevalence (BMI ≥27 kg/m^2) more than doubled from 10.5% in 2007 to 21.8% in 2018, with urban areas showing combined overweight and obesity prevalence of 50.1% [4,5]. Obesity prevalence is higher among women (25.6%) compared to men (12.8%) and is elevated among individuals with higher socioeconomic status [5], indicating this metabolic disease transcends demographic boundaries.

The pathophysiology of obesity involves dysregulated lipid metabolism and excessive adipogenesis. Elevated triglycerides promote atherogenic low-density lipoprotein (LDL) formation and reduce high-density lipoprotein (HDL), impairing

©The author(s) 2026. This article is licensed under a
Creative Commons Attribution-NonCommercial 4.0 International License

reverse cholesterol transport [6,7,8]. Excessive free fatty acid release triggers chronic inflammation and insulin resistance, creating a self-reinforcing cycle that perpetuates metabolic dysfunction [7]. Two enzymes occupy central positions in these processes: 3-hydroxy-3-methylglutaryl-coenzyme A reductase (HMGR) catalyzes the rate-limiting step in cholesterol biosynthesis [9], while glycerol-3-phosphate dehydrogenase (GPDH) plays essential roles in triglyceride synthesis and adipocyte differentiation by converting dihydroxyacetone phosphate to glycerol-3-phosphate, the backbone for triacylglycerol synthesis [10].

Statins competitively inhibit HMGR, reducing LDL by 20–50% and triglycerides by 10–20%, with demonstrated benefits in cardiovascular disease prevention [11,12,13]. However, long-term statin use is associated with adverse effects including myalgia, myositis, hepatotoxicity (3% of patients), and increased risk of new-onset diabetes mellitus [14,15,16,17]. These limitations necessitate alternative therapeutic strategies.

Eurycoma longifolia Jack (pasak bumi, tongkat ali), a medicinal plant native to Southeast Asia, has demonstrated antimalarial, antipyretic, and antidiabetic properties [18,19]. The root extract shows promise in treating hypertension and metabolic disorders [20], with studies reporting cholesterol-lowering effects in rats [21]. However, molecular interactions between *E. longifolia* bioactive compounds and key lipid metabolism enzymes (HMGR and GPDH) remain uncharacterized, and dose-response relationships require experimental validation.

This study employed molecular docking to evaluate binding interactions between seven *E. longifolia* compounds and HMGR/GPDH enzymes, with in vivo validation using diet-induced obese Wistar rats. This integrated approach elucidates molecular mechanisms and validates anti-obesity efficacy, providing scientific evidence for developing *E. longifolia* as a natural therapeutic alternative with potential multi-target metabolic benefits.

Methods

Molecular docking study

Molecular docking simulations were conducted to evaluate binding interactions between bioactive compounds from *E. longifolia* and two target enzymes: 3-hydroxy-3-methylglutaryl-coenzyme A reductase (HMGR) and glycerol-3-phosphate dehydrogenase (GPDH). The workflow encompassed protein and ligand preparation, molecular docking, validation, and visualization of binding interactions.

Three-dimensional structures of HMGR and GPDH were retrieved from the RCSB Protein Data Bank (https://www.rcsb.org/). The HMGR structure (PDB ID: 1DQ9) represents the catalytic domain of human HMG-CoA reductase complexed with HMG-CoA, while the GPDH structure (PDB ID: 1WPQ) represents glycerol-3-phosphate dehydrogenase 1 in ternary complex with NAD and dihydroxyacetone. These structures were selected based on high resolution, availability of functional data, and presence of co-crystallized control ligands that define the active site and serve as references for docking validation and binding affinity comparison. Protein preparation was performed using DockPrep tools in UCSF Chimera X version 1.8 [22]. Preparation included removal of solvent molecules and non-complexed ions, deletion of alternate conformations, standardization of residues, and replacement of incomplete side chains using the Dunbrack rotamer library [23]. Hydrogen atoms were added and Gasteiger charges were assigned to represent electrostatic interactions.

Ligand preparation

Seven bioactive compounds from *E. longifolia* and control compounds were obtained from the PubChem database (https://pubchem.ncbi.nlm.nih.gov/) in Structure-Data File (SDF) format (Table 1). For HMGR docking, HMG-CoA (native ligand), atorvastatin, and simvastatin served as controls. For GPDH docking, dihydroxyacetone phosphate (DHAP, native ligand) and metformin served as controls. Metformin was included as it inhibits mitochondrial GPDH, thereby reducing

Table 1. Compounds used as ligands for docking with HMGR and GPDH proteins, including PubChem identifiers and molecular formulas

Code	PubChem ID	Compound Name	Molecular Formula
Compound 1	13936691	Eurycomanone (Pasakbumin A)	$C_{20}H_{24}O_9$
Compound 2	3071735	Pasakbumin B	$C_{20}H_{24}O_{10}$
Compound 3	158928	10-methoxycanthin-6-one	$C_{15}H_{10}N_2O_2$
Compound 4	12004524	Piscidinol A	$C_{30}H_{50}O_4$
Compound 5	64961	β-Carboline (9H-Pyrido[3,4-b]indole	$C_{11}H_8N_2$
Compound 6	19860	3-Chloro-4-hydroxybenzoic acid	$C_7H_5ClO_3$
Compound 7	8655	Syringaldehyde	C_9H10O4
Atorvastatin	60823	Atorvastatin	$C_{33}H_{35}FN_2O_5$
Simvastatin	54454	Simvastatin	$C_{25}H_{38}O_5$
Metformin	4091	Metformin	$C_4H_{11}N_5$

cytosolic NADH/NAD^+ ratio [24]. Ligands were energy-minimized using the MMFF94 force field in Open Babel version 3.1.1 to ensure conformational stability. Protonation states were predicted at pH 7.4 using Open Babel.

Molecular docking protocol

Docking simulations were performed using AutoDock Vina version 1.2.0 [25] with exhaustiveness set to 8. The search space was defined by a grid box centered on the active site as determined by the co-crystallized control ligand position. For HMGR, the grid box was centered at X: -2.081, Y: -4.840, Z: -13.887 Å with dimensions 20.302 × 17.112 × 18.657 Å. For GPDH, the grid box was centered at X: 21.522, Y: 64.438, Z: -237.677 Å with dimensions 9.809 × 8.123 × 6.522 Å. The larger HMGR grid box accommodates the enzyme's more extensive active site pocket, while the smaller GPDH grid box reflects its more compact substrate-binding region.

Docking validation

Validation was performed by re-docking the native ligand and calculating root mean square deviation (RMSD) between the crystallographic pose and the best-scored docked pose using DockRMSD [26]. RMSD values below 2.0 Å indicate acceptable docking accuracy [27]. Validation confirmed RMSD of 1.944 Å for HMGR and 1.789 Å for GPDH.

Binding affinity analysis

AutoDock Vina calculated binding affinity as Gibbs free energy change (ΔG, kcal/mol), where more negative values indicate stronger predicted binding [28]. The dissociation constant (K_d) was calculated using the equation:

$$K_d = e^{(\Delta G/RT)}$$

where R = 1.987 cal/mol·K (gas constant) and T = 298 K (temperature). Lower K_d values indicate higher binding affinity [29].

Interaction analysis

Two-dimensional representations of ligand-protein interactions were generated using BIOVIA Discovery Studio 2021. Interactions analyzed included hydrogen bonds, hydrophobic contacts, van der Waals forces, π-π stacking, and π-alkyl interactions [30]. Amino acid residue similarity between test compounds and native ligands was calculated as:

Similarity (%) = (Number of shared residues / Total unique residues in native ligand) × 100

In vivo study

This study received ethical approval from the Research Ethics Commission of the Faculty of Medicine, Lambung Mangkurat University (approval number: 297/KEPK-FKUNLAM/VII/2019).

Table 2. Composition and nutritional content of normal diet and high-calorie high-fat diet

Ingredients	Normal Diet	High-Calorie High-Fat Diet
Commercial feed (Comfeed pars)	200 g	200 g
Wheat flour	-	100 g
Cholesterol (from duck egg yolk)	-	8 g
Pork lard	-	20 g
Water	Adjusted	Adjusted
Caloric content per 100 g	305 kcal	631 kcal
Lipid content per 100 g	5 g	30.5 g

Animals and housing

Thirty-six male Wistar rats (*Rattus norvegicus*), 8-10 weeks old, weighing 150-200 g, were obtained from the Animal Laboratory, Faculty of Medicine, Lambung Mangkurat University. Rats were housed in standard polycarbonate cages (2-3 rats per cage) under controlled conditions: temperature 22-24°C, humidity 50-60%, 12-hour light/dark cycle. All rats received food and water ad libitum throughout the study.

Diet-induced obesity model

Rats were randomly divided into two groups: normal diet control (n=6) and high-calorie high-fat diet (HCHFD, n=30). The HCHFD was prepared by mixing commercial feed (Comfeed Pars, 200 g), wheat flour (100 g), cholesterol from duck egg yolk (8 g), and pork lard (20 g), with water adjusted to achieve paste consistency. Normal diet consisted of standard commercial feed only. Diet composition is detailed in Table 2. Obesity induction was conducted for 12 weeks, with body weight monitored weekly and blood samples collected at baseline and week 12 for serum cholesterol measurement using the enzymatic colorimetric CHOD-PAP method.

Extract preparation and treatment

Eurycoma longifolia root extract was prepared by maceration of dried roots in 96% ethanol (1:10 w/v) for 72 hours, filtered, and concentrated using rotary evaporator at 50°C. Extract yield was 12.3% (w/w). Phytochemical screening confirmed the presence of alkaloids, flavonoids, terpenoids, and saponins.

Following 12-week obesity induction, rats were randomly assigned to six groups (n=6 per group): (i) normal control: normal weight rats, standard diet, distilled water vehicle; (ii) negative control: obese rats, standard diet, distilled water vehicle; (iii) T1: obese rats, standard diet, *E. longifolia* extract at 7.5 mg/kg body weight (BW); (iv) T2: obese rats, standard diet, *E. longifolia* extract at 15 mg/kg BW; (v) T3: obese rats, standard diet, *E. longifolia* extract at 22.5 mg/kg BW; P4: obese rats, standard diet, *E. longifolia* extract at 30 mg/kg BW. *E. longifolia* extract was suspended in distilled water and administered orally via gavage once daily for 4 weeks. Dose selection was based on preliminary toxicity studies showing no adverse effects up to 300 mg/kg BW.

Sample collection and measurement of intra-abdominal fat

After 4 weeks of treatment, rats were euthanized using ketamine-xylazine anesthesia. Intra-abdominal adipose tissue was carefully dissected and collected. Adipose tissue mass was measured using an analytical balance and recorded in grams.

Data analysis

Data are presented as mean ± standard deviation (SD). Normality was assessed using the Shapiro-Wilk test and homogeneity of variance using Levene's test. Differences among groups were analyzed using one-way analysis of variance (ANOVA), followed by Tukey's honestly significant difference (HSD) post hoc test for pairwise comparisons. Statistical

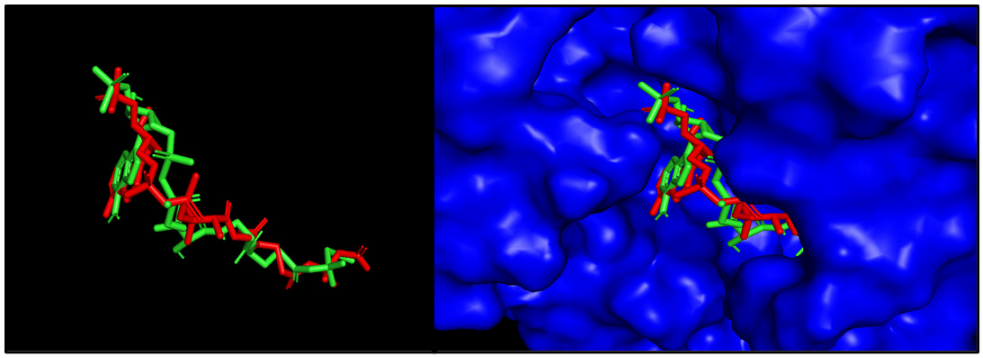

Figure 1. Validation of HMGR docking protocol. Superimposition of pre-docking control ligand (red) and post-docking control ligand (green) at the HMGR active site (blue), demonstrating RMSD of 1.944 Å.

Table 3. Binding affinity and dissociation constants of compounds with HMGR

Compounds	Binding affinity (kcal/mol)	Dissociation constant (K_d, M) at 298 K
Control (HMG-CoA)	-8.7	4.13×10^{-7}
Compound 1	-8.4	6.85×10^{-7}
Compound 2	-8.4	6.85×10^{-7}
Compound 4	-8.4	6.85×10^{-7}
Atorvastatin	-8.4	6.85×10^{-7}
Compound 3	-7.3	4.4×10^{-6}
Simvastatin	-7.0	7.3×10^{-6}
Compound 5	-6.5	1.70×10^{-5}
Compound 6	-6.1	3.34×10^{-5}
Compound 7	-5.3	1.29×10^{-4}

significance was set at $p < 0.05$. All analyses were performed using GraphPad 10.0.

Results

Molecular docking of compounds against HMGR

Docking validation confirmed protocol reliability with RMSD of 1.944 Å between the native ligand's crystallographic conformation and its best-scored docked pose (Figure 1), meeting the acceptable threshold of <2.0 Å. Both conformations occupied identical binding sites within the HMGR active site, validating the methodology for subsequent compound screening.

Binding affinities and dissociation constants for all compounds are presented in Table 3. The native ligand HMG-CoA exhibited the highest binding affinity (-8.7 kcal/mol, $K_d = 4.13 \times 10^{-7}$ M). Three *E. longifolia* compounds (Compounds 1, 2, and 4) showed binding affinities of -8.4 kcal/mol, equivalent to atorvastatin and superior to simvastatin (-7.0 kcal/mol). These three compounds shared identical K_d values (6.85×10^{-7} M) with atorvastatin, indicating comparable binding strength. Compounds 3, 5, 6, and 7 displayed progressively weaker affinities ranging from -7.3 to -5.3 kcal/mol with correspondingly higher K_d values.

Two-dimensional representations of ligand-protein interactions are shown in Figure 2. Detailed interaction analysis (Table 4) revealed that Compounds 1, 2, and 4 formed multiple hydrogen bonds with key active site residues. Compound 1 formed hydrogen bonds with Lys

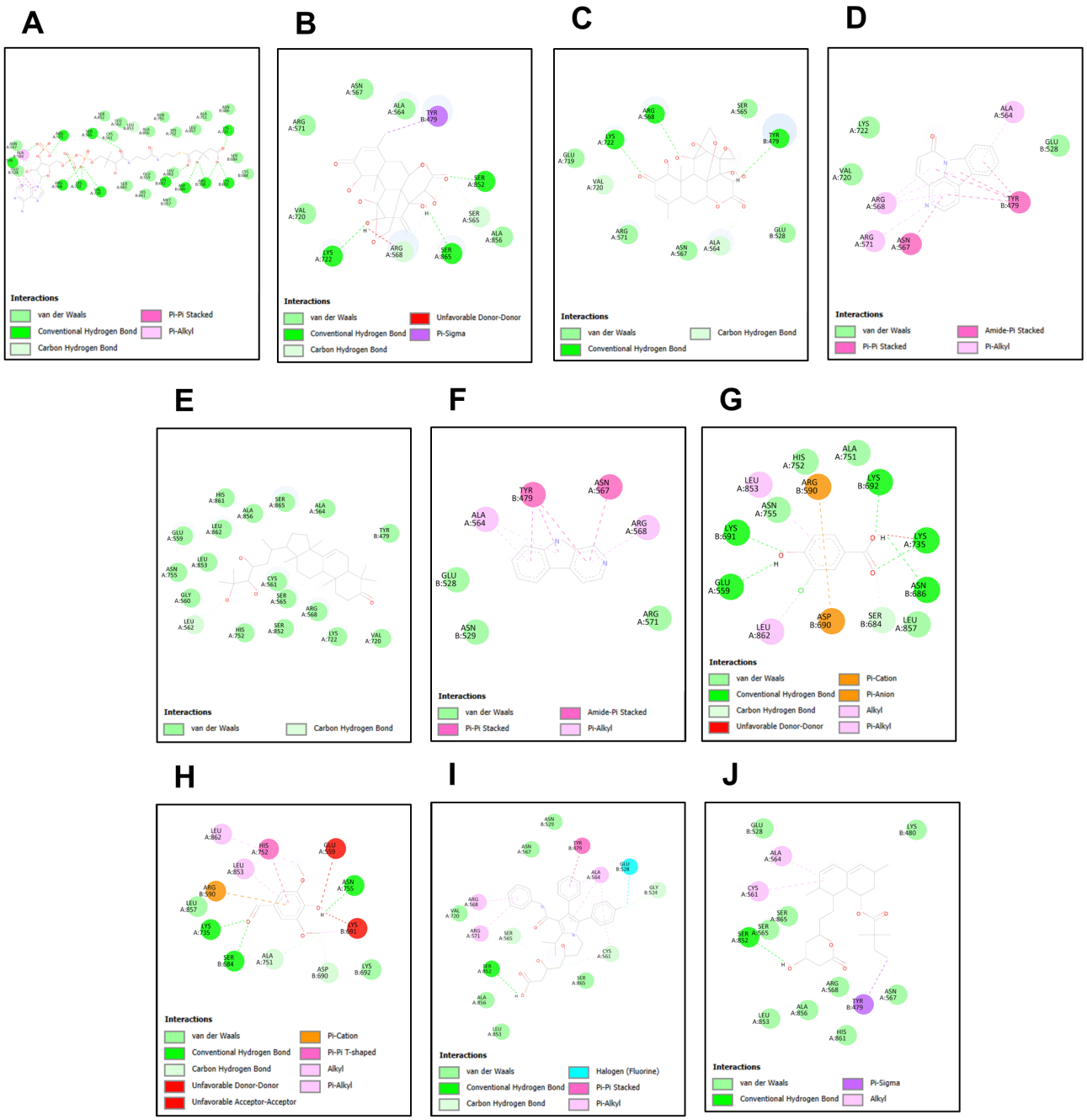

Figure 2. Two-dimensional representation of HMGR-ligand interactions. (a) HMG-CoA; (b) Compound 1; (c) Compound 2; (d) Compound 3; (e) Compound 4; (f) Compound 5; (g) Compound 6; (h) Compound 7; (i) Atorvastatin; (j) Simvastatin. Green dashed lines: hydrogen bonds; pink lines: hydrophobic interactions; light purple lines: van der Waals forces.

A:722, Ser A:865, and Ser A:852, with additional van der Waals interactions with Ala A:856, Val A:720, and Arg A:571. Compound 2 exhibited hydrogen bonding with Lys A:722, Arg A:568, and Tyr B:479. Compound 4 demonstrated extensive hydrogen bonding with 17 residues including His A:861, Ala A:856, Ser A:865, and Leu A:862.

Comparative analysis of binding site residues (Table 5) revealed that Compound 4 exhibited the highest similarity to the native ligand (46.67% shared residues), followed by Compounds 6 (43.33%) and atorvastatin (36.67%). This high residue overlap suggests that these compounds occupy similar binding regions and may function as competitive inhibitors of HMGR.

Table 4. Key amino acid interactions at the HMGR active site

Compound	Classic Hydrogen Bond	Van der Waals Bonds	Hydrophobic Bonds	Carbon-Hydrogen Bond
Control (HMG-CoA)	Tyr, Arg A:571, Ser A:565, Arg A:568, Lys A:722, Val A:720, Lys B:691, Asp B:690, Arg B:590, Lys B:692, Lys A:735	Asn A:567, Glu B:528, Ser A:852, Leu A:562, Cys A:561, Ser A:865, Ala A:856, Asn A:755, His A:752, Leu A:857, Ala A:751, Asn B:686, Glu A:559, His A:861, Leu A:862, Met B:657, Ser B:684, Cys B:688	Pi-Alkyl: Ala A:564	Leu A:853
Compound 1	Lys A:722, Ser A:865, Ser A:852	Ala A:856, Val A:720, Arg A:571, Asn A:567, Ala A:564	Pi-Sigma: Tyr B:479	Arg A:568, Ser A:565
Compound 2	Lys A:722, Arg A:568, Tyr B:479	Ser A:565, Glu A:719, Arg A:571, Asn A:567, Glu B:528	-	Val A:720, Ala A:564
Compound 4	His A:861, Ala A:856, Ser A:865, Leu A:862, Ala A:564, Leu A:853, Glu A:559, Asn A:755, Gly A:560, Cys A:561, Ser A:565, Arg A:568, His A:752, Ser A:852, Lys A:722, Val A:720	-	-	Leu A:562
Atorvastatin	Ser A:852	Ser A:865, Leu A:853, Ala A:856, Val A:720, Asn A:567, Asn B:529	Pi-Alkyl: Arg A:568, Arg A:571, Ala A:564; Pi-Pi Stacked: Tyr B:479	Ser A:565, Cys A:561, Gly B:524
Compound 3	-	Lys A:722, Val A:720, Glu B:528	Pi-Alkyl: Ala A:564, Arg A:568, Arg A:571; Pi-Pi Stacked: Asn A:567, Tyr B:479	-
Simvastatin	Ser A:852	Asn A:567, His A:861, Arg A:568, Ala A:856, Leu A:853, Ser A:565, Ser A:865, Glu B:528, Lys B:480	Pi-Sigma: Tyr B:479; Pi-Alkyl: Ala A:564, Cys A:561	-
Compound 5	-	ARG A:571, ASN B:529, GLU B:528	Pi-Pi Stacked: Asn A:567, Tyr B:479; Pi-Alkyl: Ala A:564, Arg A:568, Ala A:564	-
Compound 6	Lys A:735, Glu A:559, Lys B:629, Asn B:686, Lys B:691	His A:752, Ala A:751, Asn A:755, Leu A:857	Pi-Cation, Pi-Anion: Arg B:590, Asp B:690; Pi-Alkyl: Leu A:853, Leu A:862	Ser B:684
Compound 7	Lys A:735, Asn A:755, Ser B:684	Leu A:857, Lys B:692	Pi-Cation: Arg B:590; Pi-Pi T-Shaped: His A:752; Pi-Alkyl: Leu A:862, Leu A:853	Ala A:751, Asp B:690

Table 5. Amino acid residue similarity between test compounds and HMG-CoA at HMGR active site

Compound	Similar Residues	Similarities (%)
Compound 1	Ala A:564, Ala A:856, Arg A:568, Arg A:571, Asn A:567, Lys A:722, Ser A:565, Ser A:852, Ser A:865, Val A:720	33.33%
Compound 2	Ala A:564, Arg A:568, Arg A:571, Asn A:567, Glu B:528, Lys A:722, Ser A:565, Val A:720	26.67%
Compound 4	Ala A:564, Ala A:856, Cys A:561, His A:752, His A:861, Leu A:562, Leu A:853, Leu A:862, Lys A:722, Asn A:755, Ser A:565, Ser A:852, Ser A:865, Val A:720	46.67%
Atorvastatin	Ala A:564, Ala A:856, Arg A:568, Arg A:571, Asn A:567, Cys A:561, Leu A:853, Ser A:565, Ser A:852, Ser A:865, Val A:720	36.67%
Compound 3	Ala A:564, Arg A:568, Asn A:567, Glu B:528, Lys A:722, Val A:720	20%
Simvastatin	Ala A:856, Arg A:568, Asn A:567, Cys A:561, His A:861, Leu A:853, Ser A:565, Ser A:852, Ser A:865	30%
Compound 5	Ala A:564, Arg A:568, Arg A:571, Asn A:567, Glu B:528	16.67%
Compound 6	Ala A:751, Arg B:590, Asn A:755, Asn B:686, Asp B:690, Glu A:559, His A:752, Leu A:853, Leu A:857, Leu A:862, Lys A:735, Lys B:691, Ser B:684	43.33%
Compound 7	Arg B:590, Asn A:755, His A:752, Leu A:853, Leu A:857, Leu A:862, Lys B:692, Ser B:684	26.67%

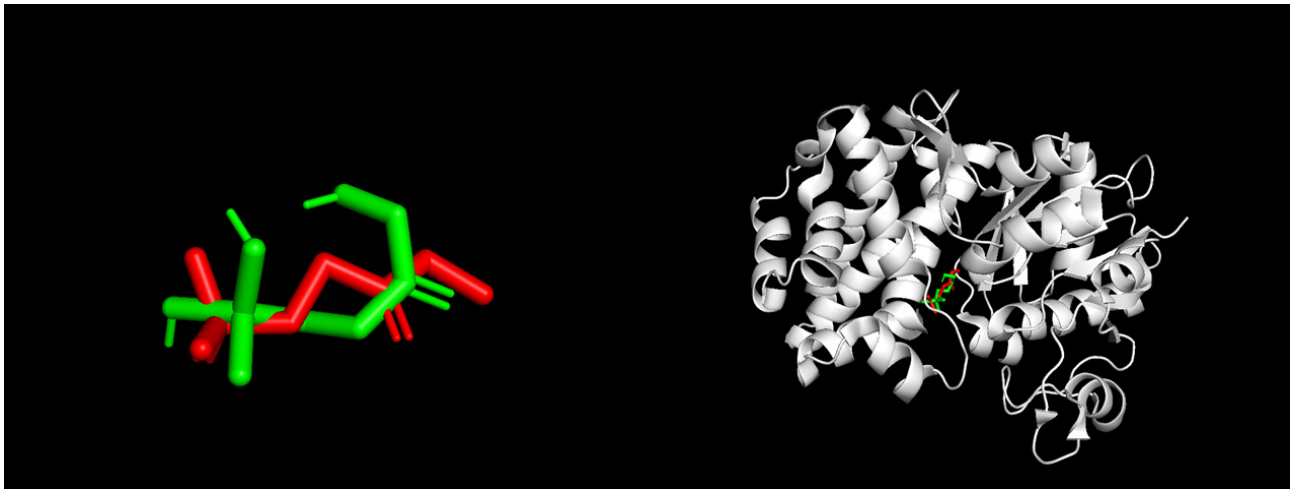

Figure 3. Validation of GPDH docking protocol. Superimposition of pre-docking control ligand (red) and post-docking control ligand (green) at the GPDH active site (gray), demonstrating RMSD of 1.789 Å.

Table 6. Binding affinity and dissociation constants of compounds with GPDH

Compound	Binding Affinity (kcal/mol)	Dissociation Constant (Kd, M) at 298 K
Compound 3	-6.5	1.70×10^{-5}
Compound 5	-6.2	2.82×10^{-5}
Compound 6	-6.0	3.95×10^{-5}
Compound 7	-5.8	5.54×10^{-5}
Control (DHAP)	-5.3	1.29×10^{-4}
Metformin	-5.0	2.14×10^{-4}
Compound 2	8.0	Non-spontaneous
Compound 1	11.8	Non-spontaneous
Compound 4	55.2	Non-spontaneous

Molecular docking of compounds with GPDH

GPDH docking validation yielded RMSD of 1.789 Å (Figure 3), confirming protocol reliability. The native ligand DHAP occupied identical positions before and after docking, validating the methodology.

Binding affinities and dissociation constants for GPDH interactions are presented in Table 6. Four *E. longifolia* compounds (3, 5, 6, and 7) exhibited stronger binding than both DHAP (-5.3 kcal/mol) and metformin (-5.0 kcal/mol). Compound 3 demonstrated the highest affinity (-6.5 kcal/mol, $K_d = 1.70 \times 10^{-5}$ M), representing 13-fold stronger binding than metformin. Compounds 5, 6, and 7 showed affinities of -6.2, -6.0, and -5.8 kcal/mol, respectively. Conversely, Compounds 1, 2, and 4 showed positive ΔG values (11.8, 8.0, and 55.2 kcal/mol, respectively), indicating thermodynamically unfavorable binding to GPDH, suggesting selectivity for HMGR over GPDH.

Two-dimensional visualizations of GPDH binding interactions are shown in Figure 4. Interaction analysis (Table 7) revealed that Compound 3 formed hydrogen bonds with Arg A:269 and exhibited π-cation and π-anion interactions with Lys A:204 and Asp A:260. Compound 5 formed hydrogen bonds with Asn A:151 and multiple π-interactions. Compounds 6 and 7 showed hydrogen bonding but also displayed unfavorable donor-donor interactions, which may slightly reduce binding stability despite overall favorable affinity.

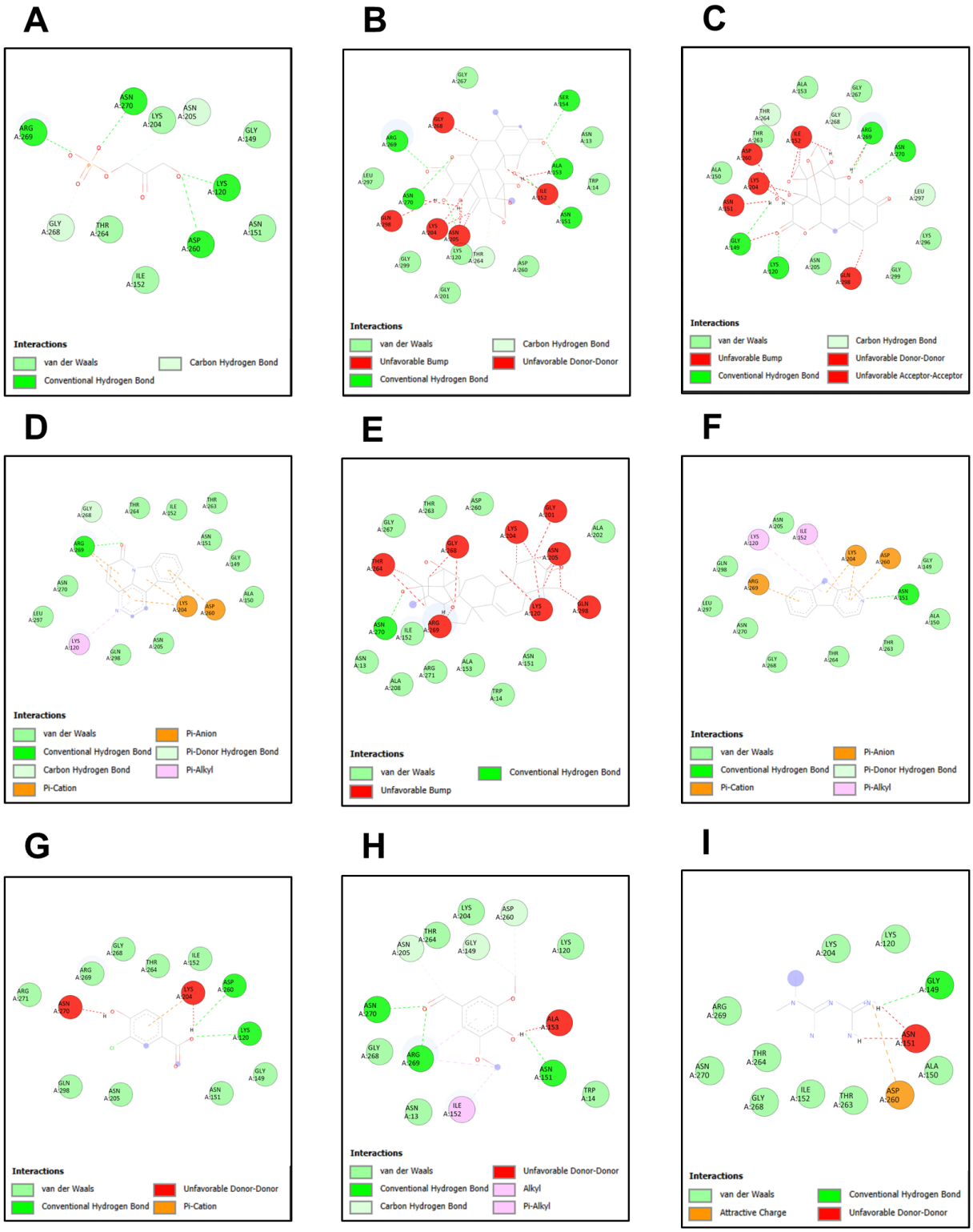

Figure 4. Two-dimensional representation of GPDH-ligand interactions. (a) DHAP; (b) Compound 1; (c) Compound 2; (d) Compound 3; (e) Compound 4; (f) Compound 5; (g) Compound 6; (h) Compound 7; (i) Metformin. Green dashed lines: hydrogen bonds; pink: hydrophobic interactions; orange: unfavorable interactions.

Table 7. Key amino acid interactions at the GPDH active site

Compound	Classic Hydrogen Bond	Van der Waals Bonds	Hydrophobic Bonds	Carbon-Hydrogen Bond	Others
Compound 3	Arg A:269	Asn A:270, Leu A:297, Gln A:298, Asn A:205, Ala A:150, Gly A:149, Asn A:151, Thr A:263, Ile A:152, Thr A:264	Pi-Cation and Pi-Anion: Lys A:204, Asp A:260; Pi-Donor Hydrogen Bond: Gly A:268; Pi-Alkyl: Lys A:120	Gly A:268	-
Compound 5	Asn A:151	Gln A:298, Leu A:297, Asn A:270, Gly A:268, Thr A:264, Thr A:263, Ala A:150, Gly A:149, Asn A:205	Pi-Cation and Pi-Anion: Arg A:269, Lys A:204, Asp A:260; Pi-Alkyl: Lys A:120, Ile A:152; Pi-Donor Hydrogen Bond: Gly A:268	-	-
Compound 6	Asp A:260, Lys A:120	Gln A:298, Asn A:205, Asn A:151, Gly A:149, Ile A:152, Thr A:264, Gly A:268, Arg A:269, Arg A:271	-	-	Unfavorable Donor-Donor: Asn A:270, Lys A:204
Compound 7	Arg A:269, Asn A:151	Gly A:268, Asn A:13, Trp A:14, Lys A:120, Lys A:204, Thr A:264	Pi-Alkyl: Ile A:152	Asn A:205, Gly A:149, Asp A:260	Unfavorable Donor-Donor: Ala A:153
Control (DHAP)	Arg A:269, Asn A:270, Lys A:120, Asp A:260	Thr A:264, Ile A:152, Asn A:151, Gly A:149, Lys A:204	-	Gly A:268, Asn A:265	-
Metformin	Gly A:149	Arg A:269, Asn A:270, Thr A:264, Gly A:268, Ile A:152, Thr A:263, Ala A:150, Lys A:204, Lys A:120	-	-	Attractive Charge: Asp A:260; Unfavorable Donor-Donor: Asn A:151
Compound 2	Gly A:149, Lys A:120, Arg A:269, Asn A:270	Ala A:150, Asn A:205, Gly A:299, Lys A:296, Gly A:267, Ala A:153, Thr A:263	-	Thr A:264, Gly A:268, Leu A:297	Unfavorable Donor-Donor And Unfavorable Bump: Gln A:298, Asn A:151, Lys A:204, Asp A:260, Ile A:152
Compound 1	Arg A:269, Asn A:270, Ser A:154, Ala A:153, Asn A:151	Leu A:297, Gly A:299, Lys A:120, Gly A:201, Asp A:260, Trp A:14, Asn A:13, Gly A:267	-	Thr A:264	Unfavorable Donor-Donor And Unfavorable Bump: Gly A:268, Gln A:298, Lys A:204, Asn A:205, Ile A:152
Compound 4	Asn A:270	Asn A:13, Ala A:208, Ile A:152, Arg A:271, Ala A:153, Trp A:14, Asn A:151, Ala A:202, Asp A:260, Thr A:263, Gly A:267	-	-	Unfavorable Bump: Thr A:264, Arg A:269, Gly A:268, Lys A:204, Gly A:201, Asn A:205, Lys A:120, Gln A:298

Table 8. Amino acid residue similarity between test compounds and DHAP at GPDH active site

Compound	Similar Residues	Similarities (%)
Compound 3	Arg A:269, Asn A:270, Asn A:151, Ile A:152, Thr A:264, Lys A:204, Asp A:260, Gly A:268, Lys A:120, Gly A:149	90.91%
Compound 5	Asn A:151, Asn A:270, Gly A:268, Thr A:264, Gly A:149, Arg A:269, Lys A:204, Asp A:260, Lys A:120, Ile A:152	90.91%
Compound 6	Asp A:260, Lys A:120, Asn A:151, Gly A:149, Ile A:152, Thr A:264, Gly A:268, Arg A:269, Asn A:270, Lys A:204	90.91%
Compound 7	Arg A:269, Asn A:151, Gly A:268, Lys A:120, Lys A:204, Thr A:264, Ile A:152, Gly A:149, Asp A:260	81.82%
Metformin	Gly A:149, Arg A:269, Asn A:270, Thr A:264, Gly A:268, Ile A:152, Lys A:204, Lys A:120	72.73%
Compound 2	Gly A:149, Lys A:120, Arg A:269, Asn A:270, Thr A:264, Gly A:268, Asn A:151, Lys A:204, Asp A:260, Ile A:152	90.91%
Compound 1	Arg A:269, Asn A:270, Asn A:151, Lys A:120, Asp A:260, Thr A:264, Gly A:268, Lys A:204, Ile A:152	81.82%
Compound 4	Asn A:270, Ile A:152, Asn A:151, Asp A:260, Thr A:264, Arg A:269, Gly A:268, Lys A:204, Lys A:120	81.82%

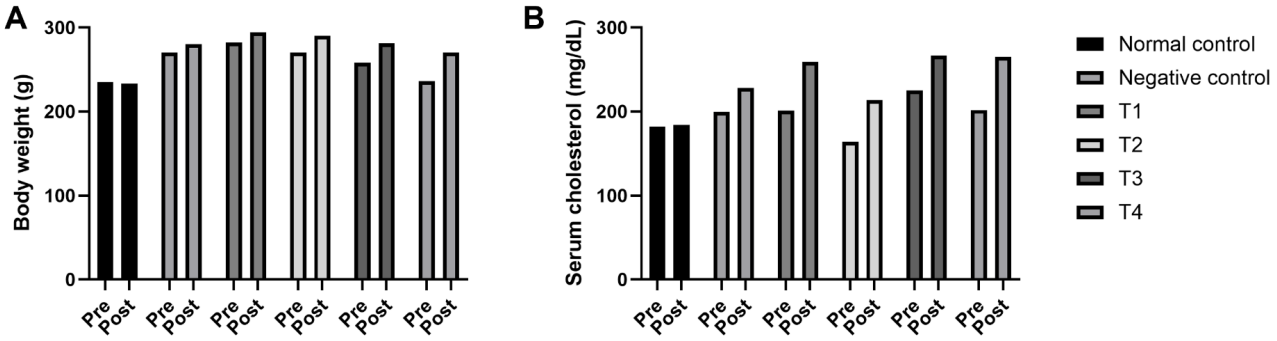

Figure 5. Effects of *E. longifolia* extract on body weight and serum cholesterol levels in high carbohydrate high fat diet (HCHFD) induced obese rats. Body weight (A) and serum cholesterol (B) measured before (Pre) and after (Post) 12-week HCHFD induction. Treatment groups: Normal control (normal weight rats, standard diet), Negative control (obese rats, standard diet), and T1-T4 (obese rats treated with *E. longifolia* extract at 7.5, 15, 22.5, and 30 mg/kg body weight, respectively). Extract was administered orally once daily for 4 weeks following HCHFD induction.

Comparative analysis (Table 8) revealed that Compounds 2, 3, 5, and 6 exhibited exceptionally high residue similarity with DHAP (90.91% shared residues), substantially higher than metformin (72.73%). This extensive overlap indicates these compounds bind at the native substrate site and likely function as competitive GPDH inhibitors.

In vivo effects of *Eurycoma longifolia* Jack extract

Body weight and serum cholesterol levels before and after 12-week HCHFD induction are presented in Figure 5. Normal control group (normal control) maintained stable body weight and cholesterol levels, while all HCHFD-fed groups showed significant increases in both parameters ($p < 0.01$), confirming successful obesity induction.

After four weeks of *Eurycoma longifolia* extract treatment, body weight and intra-abdominal fat mass are presented in Table 9. Negative control exhibited significantly elevated intra-abdominal fat compared to normal control ($p < 0.001$), confirming the obesity phenotype. *Eurycoma longifolia* extract treatment produced dose-dependent reductions in intra-abdominal fat across all treatment groups (28.3-64.9% reduction vs negative control). The

Table 9. Body weight and intra-abdominal fat mass after four weeks of *Eurycoma longifolia* Jack treatment

Parameter	Normal control	Negative control	T1	T2	T3	T4
Average body weight (g)	275	280	282	281.67	270	258.33
Intra-abdominal fat (g)	3.133 ± 0.931	10.080 ± 0.870	7.224 ± 0.989	5.601 ± 0.588	5.019 ± 0.308	3.540 ± 0.947

Data presented as mean ± SD (n=6). T1-T4: *Eurycoma longifolia* extract treatment at 7.5, 15, 22.5, and 30 mg/kg BW, respectively.

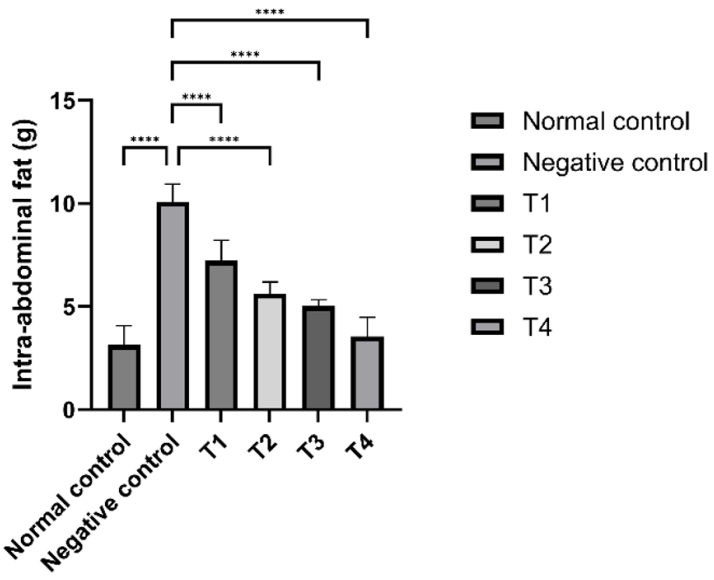

Figure 6. Dose-dependent effect of *Eurycoma longifolia* extract on intra-abdominal fat mass. Bars represent mean ± SD (n=6). Different letters indicate significant differences ($p < 0.05$, Tukey's HSD). One-way ANOVA: $F(5,30) = 87.34$, $p < 0.001$. T1-T4: *Eurycoma longifolia* extract treatment at 7.5, 15, 22.5, and 30 mg/kg BW, respectively.

highest dose (T4, 30 mg/kg) achieved complete normalization of visceral adiposity, with fat levels not significantly different from normal control ($p = 0.342$). One-way ANOVA confirmed significant differences among groups ($F = 87.34$, $df = 5,30$, $p < 0.001$), as visualized in Figure 6.

Discussion

This study demonstrates that bioactive compounds from *Eurycoma longifolia* possess dual therapeutic potential targeting both cholesterol biosynthesis and adipogenesis through inhibition of HMGR and GPDH enzymes. Molecular docking simulations revealed that eurycomanone, pasakbumin B, and piscidinol A exhibit binding affinities to HMGR equivalent to atorvastatin (-8.4 kcal/mol), while 10-methoxycanthin-6-one, β-carboline, 3-chloro-4-hydroxybenzoic acid, and syringaldehyde demonstrate superior binding to GPDH compared to metformin. In vivo validation confirmed significant, dose-dependent reduction in intra-abdominal fat following *E. longifolia* root extract treatment, with the highest dose achieving complete normalization of visceral adiposity.

HMGR catalyzes the rate-limiting step in cholesterol biosynthesis, converting HMG-CoA to mevalonate, and serves as the primary molecular target of statins [31]. While statins effectively reduce cardiovascular disease risk, long-term use is associated with myalgia, hepatotoxicity, and increased diabetes risk [15–18, 32]. Our docking results demonstrate that eurycomanone, pasakbumin B, and piscidinol A exhibited binding affinities equivalent to atorvastatin with identical dissociation constants ($K_d = 6.85 \times 10^{-7}$ M). These compounds engaged key active site residues overlapping with atorvastatin, including Ser A:565, Arg A:568, Ala A:856, and Ala A:564. Piscidinol A showed the highest

residue similarity to the native ligand (46.67%), suggesting competitive inhibition potential through occupation of the CoA and HMG binding subsites [31]. These findings align with previous studies demonstrating natural compounds successfully inhibit HMGR [33,34]. The lipid-lowering effects of *E. longifolia* in obese mice reported by Triawanti et al. [35] provide experimental support for the predicted HMGR inhibitory activity observed in our computational analysis.

GPDH plays crucial roles in triglyceride biosynthesis and adipocyte differentiation by converting dihydroxyacetone phosphate to glycerol-3-phosphate, the backbone for triacylglycerol synthesis [10]. Our docking results show 10-methoxycantin-6-one, β-carboline, 3-chloro-4-hydroxybenzoic acid, and syringaldehyde exhibited stronger binding affinities to GPDH than both DHAP and metformin, with 10-methoxycanthin-6-one demonstrating 13-fold stronger binding than metformin. These compounds shared approximately 90.91% residue similarity with DHAP, substantially higher than metformin's 72.73%, indicating competitive inhibition potential. They engaged key active site residues including Arg A:269, Asn A:270, Thr A:264, Lys A:204, and Asp A:260. The anti-adipogenic potential is supported by Balan et al. [36], who demonstrated that *E. longifolia* extract inhibited lipid accumulation and decreased PPARγ and C/EBPα expression in 3T3-L1 adipocytes. Enhanced GPDH activity has been associated with increased triglyceride accumulation and obesity development [37], making this enzyme a rational therapeutic target for metabolic disorders.

Notably, eurycomanone, pasakbumin B, and piscidinol A showed strong HMGR binding but thermodynamically unfavorable GPDH binding (positive ΔG values), while 10-methoxycanthin-6-one, β-carboline, 3-chloro-4-hydroxybenzoic acid, and syringaldehyde demonstrated the opposite selectivity pattern. This selectivity suggests different structural features confer enzyme specificity, and that *E. longifolia* root extracts containing multiple compounds could provide synergistic effects by simultaneously targeting complementary pathways in lipid metabolism. This multi-target profile distinguishes natural product-based therapeutics from single-target pharmaceutical interventions and may explain the traditional efficacy of whole plant extracts.

Our in vivo study employed a validated diet-induced obesity model [38] and demonstrated significant, dose-dependent reductions in intra-abdominal fat following *E. longifolia* root extract treatment. The negative control group exhibited 3.2-fold higher intra-abdominal fat compared to normal controls, confirming the obesity phenotype. Extract treatment at doses ranging from 7.5 to 30 mg/kg BW progressively reduced visceral fat by 28.3% to 64.9%, with the highest dose achieving complete normalization. Visceral fat reduction has important clinical implications as this adipose depot releases inflammatory cytokines (TNF-α, IL-6) that contribute to insulin resistance, dyslipidemia, and cardiovascular risk [39]. Zhang et al. [40] demonstrated that *E. longifolia* decreased lipid metabolite expression while upregulating β-oxidation products in obese mice, indicating dual action through inhibiting lipogenesis and promoting lipolysis. This systemic metabolic reprogramming, potentially involving AMPK signaling and autophagy pathways [41], may explain the potent fat-reducing effects observed in our study. The dose-dependent response and achievement of normal adiposity levels at the highest dose without apparent adverse effects suggest a favorable therapeutic window for *E. longifolia* root extract.

The integration of computational and experimental approaches in this study provides complementary evidence for the anti-obesity potential of *E. longifolia*. Molecular docking identified specific compounds and mechanisms, while in vivo experiments validated the physiological efficacy of whole extract. However, several limitations warrant acknowledgment. Molecular docking provides computational predictions but does not confirm actual inhibitory activity; in vitro enzymatic assays with purified HMGR and GPDH are essential to validate predictions and determine IC_{50} values. We did not directly measure enzyme activities in tissues, limiting mechanistic confirmation at the molecular level. The bioavailability and pharmacokinetics of individual compounds remain unknown, as some

may undergo extensive first-pass metabolism or exhibit poor absorption despite favorable binding profiles. The relatively short treatment duration (4 weeks) and use of rodent models limit direct extrapolation to chronic human obesity management.

Future research should address these limitations through comprehensive investigations. In vitro enzymatic assays using purified HMGR and GPDH with individual compounds are needed to validate predicted inhibition and determine IC_{50} values. Cell-based assays in hepatocytes and adipocytes would confirm effects on cholesterol and triglyceride synthesis. Pharmacokinetic studies are essential to determine absorption, distribution, metabolism, and excretion profiles of bioactive compounds. Comprehensive toxicity evaluation including hepatic function, renal function, and muscle enzymes should be conducted across extended treatment periods to establish safety profiles. Multi-omics approaches (transcriptomics, proteomics, lipidomics, metabolomics) could provide systems-level understanding of metabolic reprogramming mechanisms. Bioassay-guided fractionation and structure-activity relationship studies could identify the most potent compounds and guide optimization through medicinal chemistry approaches. Preliminary clinical trials in human subjects with obesity would be essential to determine efficacy, optimal dosing, and safety in target populations.

The growing obesity prevalence, particularly in urbanizing regions like Southeast Asia where combined overweight and obesity affects half the urban population, creates urgent need for safe, effective therapeutic interventions [4,5]. Natural product-based therapeutics offer potential advantages including multi-target activity and potentially favorable safety profiles based on traditional use. If validated through additional studies, *E. longifolia*-based therapeutics could serve as alternatives or adjuncts to conventional treatments. For patients experiencing statin intolerance, *E. longifolia* compounds targeting HMGR might offer alternative means of addressing dyslipidemia. The multi-target nature—simultaneously addressing cholesterol biosynthesis and adipogenesis—could provide more comprehensive metabolic benefits than single-target interventions. Combination therapy approaches might enable dose reduction of pharmaceutical agents, potentially minimizing adverse effects while maintaining therapeutic efficacy. However, rigorous safety assessment including toxicology studies and evaluation of potential drug-drug interactions is essential before clinical development.

This study provides scientific foundation for developing *E. longifolia* as an evidence-based natural therapeutic for obesity management. Our findings reveal complementary compound groups within the plant: eurycomanone, pasakbumin B, and piscidinol A target HMGR (reducing cholesterol synthesis), while 10-methoxycanthin-6-one, β-carboline, 3-chloro-4-hydroxybenzoic acid, and syringaldehyde target GPDH (suppressing adipogenesis). This dual-pathway mechanism may contribute to the traditional medicinal use of *E. longifolia* for metabolic disorders and supports further development as a multi-target therapeutic agent. The dose-dependent efficacy and complete normalization of visceral adiposity without apparent toxicity provide encouraging preliminary evidence, though extensive safety evaluation and human clinical trials remain essential prerequisites for therapeutic application.

Conclusion

This integrated study demonstrates that *Eurycoma longifolia* compounds possess dual inhibitory potential against HMGR and GPDH enzymes. Eurycomanone, pasakbumin B, and piscidinol A exhibited binding affinities equivalent to atorvastatin for HMGR, while 10-methoxycanthin-6-one, β-carboline, 3-chloro-4-hydroxybenzoic acid, and syringaldehyde showed superior binding to GPDH compared to metformin. In vivo validation confirmed dose-dependent reduction in visceral adiposity (28.3-64.9%), with complete normalization at 30 mg/kg BW. These findings provide scientific evidence supporting *E. longifolia* as a multi-target natural therapeutic for obesity management.

Acknowledgment

Not applicable.

Funding

Not applicable.

Author contributions

Conceptualization: T. and D.I.A. Supervision: T. methodology: D.I.A, T. and H.R.R ; in silico simulation: D.I.A. and M.A.R.; in vivo experimental: T. and D.I.A., Writing-draft: D.I.A and H.R.R., Writing-review & editing: D.I.A, H.R.R., and T. All authors have read and approved to the published version of the manuscript

Declaration of interest

The authors declare that none of them has any conflict of interest with any private, public or academic party related to the information contained in this manuscript

Received: December 12, 2025
Revised: February 4, 2026
Accepted: February 5, 2026
Published: February 6, 2026

References

1. Emmerich SD, Cheryl DV, Fryar MSP, Bryan S, Ogden CL. Obesity and severe obesity prevalence in adults: United States, August 2021-August 2023. National Center for Health Statistics; 2024. https://doi.org/10.15620/cdc/159281
2. World Health Organization. World Obesity Day 2022 - accelerating action to stop obesity. WHO; 2022. Available from: https://www.who.int/news/item/04-03-2022-world-obesity-day-2022-accelerating-action-to-stop-obesity
3. Lui DTW, Ako J, Dalal J, Fong A, Fujino M, Horton A, et al. Obesity in the Asia-Pacific region: current perspectives. J Asian Pac Soc Cardiol. 2024;3:e21. https://doi.org/10.15420/japsc.2023.68
4. Ferdiana AR, Arfines PP, Aryastami NK. Obesity in urban Indonesia: evidence from the 2007 and 2018 Basic Health Research. Med J Indones. 2024;33:119-27. https://doi.org/10.13181/mji.oa.247183
5. Roemling C, Qaim M. Disparities in obesity rates among adults: analysis of 514 districts in Indonesia. BMC Public Health. 2022;22:1843. https://doi/org/10.1186/s12889-022-14224-1
6. Vekic J, Zeljkovic A, Stefanovic A, Jelic-Ivanovic Z, Spasojevic-Kalimanovska V. Obesity and dyslipidemia. Metabolism. 2019;92:71-81. https://doi.org/10.1016/j.metabol.2018.11.005
7. Klop B, Elte JWF, Cabezas MC. Dyslipidemia in obesity: mechanisms and potential targets. Nutrients. 2013;5:1218-40. https://doi.org/10.3390/nu5041218
8. Bays HE, Kirkpatrick C, Maki KC, Toth PP, Morgan RT, Tondt J, et al. Obesity, dyslipidemia, and cardiovascular disease: a joint expert review from the Obesity Medicine Association and the National Lipid Association 2024. Obes Pillars. 2024;10:100108. https://doi.org/10.1016/j.obpill.2024.100108
9. Kotyla P. The role of 3-hydroxy-3-methylglutaryl coenzyme A reductase inhibitors (statins) in modern rheumatology. Ther Adv Musculoskelet Dis. 2010;2:257-69. https://doi.org/10.1177/1759720X10384307
10. Oh S, Mai XL, Kim J, de Guzman ACV, Lee JY, Park S. Glycerol 3-phosphate dehydrogenases (1 and 2) in cancer and other diseases. Exp Mol Med. 2024;56(5):1066-79. https://doi.org/10.1038/s12276-024-01222-1
11. Jiang SY, Li H, Tang JJ, Wang J, Luo J, Liu B, et al. Discovery of a potent HMG-CoA reductase degrader that eliminates statin-induced reductase accumulation and lowers cholesterol. Nat Commun. 2018;9:5138. https://doi.org/10.1038/s41467-018-07590-3
12. Taylor F, Huffman MD, Macedo AF, Moore THM, Burke M, Davey Smith G, et al. Statins for the primary prevention of cardiovascular disease. Cochrane Database Syst Rev. 2013;2013:CD004816. https://doi.org/10.1002/14651858.CD004816.pub5
13. Odden MC, Pletcher MJ, Coxson PG, Thekkethala D, Guzman D, Heller D, et al. Cost-effectiveness and population impact of statins for primary prevention in adults aged 75 years or older in the United States. Ann Intern Med. 2015;162:533-41. https://doi.org/10.7326/M14-1430
14. Ward NC, Watts GF, Eckel RH. Statin toxicity. Circ Res. 2019;124:328-50. https://doi.org/10.1161/CIRCRESAHA.118.312782
15. Pedro-Botet J, Núñez-Cortés JM, Flores JA, Rius J. Muscle symptoms related with statin therapy in general practice. Atherosclerosis. 2015;241:e197. https://doi.org/10.1016/j.atherosclerosis.2015.04.957
16. Ramkumar S, Raghunath A, Raghunath S. Statin therapy: review of safety and potential side effects. Acta Cardiol Sin. 2016;32:631-9. https://doi.org/10.6515/acs20160611a
17. Russo MW, Hoofnagle JH, Gu J, Fontana RJ, Barnhart H, Kleiner DE, et al. Spectrum of statin hepatotoxicity: experience of the drug-induced liver injury network. Hepatology. 2014;60:679-86. https://doi.org/10.1002/hep.27157
18. Bang CN, Okin PM. Statin treatment, new-onset diabetes, and other adverse effects: a systematic review. Curr Cardiol Rep. 2014;16:461. https://doi.org/10.1007/s11886-013-0461-4
19. Kuo PC, Damu AG, Lee KH, Wu TS. Cytotoxic and antimalarial constituents from the roots of Eurycoma

longifolia. Bioorg Med Chem. 2004;12:537-44. https://doi.org/10.1016/j.bmc.2003.11.017

20. Nurani LH, Kumalasari E, Rohman A, Widyarini S. Capsule formulation of ethanolic extract of pasak bumi (Eurycoma longifolia Jack) and its effect on human health vital signs. Tradit Med J. 2017;22:91-6. https://doi.org/10.22146/tradmedj.27919
21. Nurmeilis N, Woro DA, Soemiati A, Khoirunisa A. Diuretic activity and acute toxicity of combination Eurycoma longifolia extract and irbesartan. Indones J Pharm Sci. 2015;2. https://doi.org/10.15416/ijpst.v2i1.7805
22. Meng EC, Goddard TD, Pettersen EF, Couch GS, Pearson ZJ, Morris JH, Ferrin TE. UCSF ChimeraX: tools for structure building and analysis. Protein Sci. 2023;32(11):e4792. https://doi.org/10.1002/pro.4792
23. Shapovalov MV, Dunbrack RL. A smoothed backbone-dependent rotamer library for proteins derived from adaptive kernel density estimates and regressions. Structure. 2011;19(6):844-58. https://doi.org/10.1016/j.str.2011.03.019
24. Foretz M, Guigas B, Viollet B. Understanding the glucoregulatory mechanisms of metformin in type 2 diabetes mellitus. Nat Rev Endocrinol. 2019;15(10):569-89. https://doi.org/10.1038/s41574-019-0242-2
25. Eberhardt J, Santos-Martins D, Tillack AF, Forli S. AutoDock Vina 1.2.0: new docking methods, expanded force field, and python bindings. J Chem Inf Model. 2021;61(8):3891-8. https://doi.org/10.1021/acs.jcim.1c00203
26. Bell EW, Zhang Y. DockRMSD: an open-source tool for atom mapping and RMSD calculation of symmetric molecules through graph isomorphism. J Cheminform. 2019;11(1):40. https://doi.org/10.1186/s13321-019-0362-7
27. Vittorio S, Lunghini F, Morerio P, Gadioli D, Orlandini S, Silva P, Martinovic J, Pedretti A, Bonanni D, Del Bue A, Palermo G. Addressing docking pose selection with structure-based deep learning: recent advances, challenges and opportunities. Comput Struct Biotechnol J. 2024;23:2141-51. https://doi.org/10.1016/j.csbj.2024.04.042
28. Schön A, Madani N, Smith AB, Lalonde JM, Freire E. Some binding-related drug properties are dependent on thermodynamic signature. Chem Biol Drug Des. 2011;77(3):161-5. https://doi.org/10.1111/j.1747-0285.2010.01073.x
29. Singh S, Singh DB, Gautam B, Singh A, Yadav N. Pharmacokinetics and pharmacodynamics analysis of drug candidates. In: Bioinformatics. Academic Press; 2022. p. 305-16. https://doi.org/10.1016/B978-0-323-89775-4.00001-8
30. Mohanty M, Mohanty PS. Molecular docking in organic, inorganic, and hybrid systems: a tutorial review. Monatshefte Für Chemie. 2023;154(7):683-707. https://doi.org/10.1007/s00706-023-03076-1
31. Gesto DS, Pereira CMS, Cerqueira NMFS, Sousa SF. An atomic-level perspective of HMG-CoA-reductase: the target enzyme to treat hypercholesterolemia. Molecules. 2020;25(17):3891. https://doi.org/10.3390/molecules25173891
32. Laakso M, Fernandes Silva L. Statins and risk of type 2 diabetes: mechanism and clinical implications. Front Endocrinol. 2023;14:1239335. https://doi.org/10.3389/fendo.2023.1239335
33. Lin SH, Huang KJ, Weng CF, Shiuan D. Exploration of natural product ingredients as inhibitors of human HMG-CoA reductase through structure-based virtual screening. Drug Des Dev Ther. 2015;9:3313-24. https://doi.org/10.2147/DDDT.S84641
34. Ruan J, Li Z, Zhang Y, Chen Y, Liu M, Han L, Zhang Y, Wang T. Bioactive constituents from the roots of Eurycoma longifolia. Molecules. 2019;24(17):3157. https://doi.org/10.3390/molecules24173157
35. Triawanti, Sanyoto DD, Rosida A, Nur'amin HW, Jangkang GG, Airlangga DI. The effect of pasak bumi (Eurycoma longifolia Jack) ethanol extract on the lipid profile of the rats was induced high-calorie high-fat diet. IOSR J Pharm Biol Sci. 2022;17(1 Suppl 2):1-7. https://doi.org/10.9790/3008-1701020107
36. Balan D, Chan KL, Murugan D, AbuBakar S, Wong PF. Antiadipogenic effects of a standardized quassinoids-enriched fraction and eurycomanone from Eurycoma longifolia. Phytother Res. 2018;32(7):1332-45. https://doi.org/10.1002/ptr.6069
37. Swierczynski J, Zabrocka L, Goyke E, Raczynska S, Adamonis W, Sledzinski Z. Enhanced glycerol 3-phosphate dehydrogenase activity in adipose tissue of obese humans. Mol Cell Biochem. 2003;254(1-2):55-9. https://doi.org/10.1023/A:1027332523114
38. Hariri N, Thibault L. High-fat diet-induced obesity in animal models. Nutr Res Rev. 2010;23(2):270-99. https://doi.org/10.1017/S0954422410000168
39. Cesaro A, De Michele G, Fimiani F, Acerbo V, Scherillo G, Signore G, Rotolo FP, Scialla F, Raucci G, Panico D, Gragnano F. Visceral adipose tissue and residual cardiovascular risk: a pathological link and new therapeutic options. Front Cardiovasc Med. 2023;10:1187735. https://doi.org/10.3389/fcvm.2023.1187735
40. Zhang D, Zheng W, Li X, Liang G, Ye N, Liu Y, Li A, Liu X, Zhang R, Cheng J, Yang H. Investigation of obesity-alleviation effect of Eurycoma longifolia on mice fed with a high-fat diet through metabolomics revealed enhanced decomposition and inhibition of accumulation of lipids. J Proteome Res. 2021;20(5):2714-24. https://doi.org/10.1021/acs.jproteome.1c00015
41. An H, Jang Y, Choi J, Hur J, Kim S, Kwon Y. New insights into AMPK as a potential therapeutic target in metabolic dysfunction-associated steatotic liver disease and hepatic fibrosis. Biomolecules Therapeutics. 2024;33(1):18. https://doi.org/10.4062/biomolther.2024.177